BNL-209093-2018-TECH
CBETA/028

First tests of electron beam transport in the CBETA S1 splitter line

E. Biddulph-West, S. Peggs

September 2018

Collider Accelerator Department
Brookhaven National Laboratory

U.S. Department of Energy
USDOE Office of Science (SC), Nuclear Physics (NP) (SC-26)

DISCLAIMER

First Tests of Electron Beam Transport in the CBETA S1 Splitter Line

Eric Biddulph-West
CLASSE, Cornell University, Ithaca, New York, 14853

In May, 2018, the Cornell-University Brookhaven-National-Laboratory Energy-Recovery-Linac Test Accelerator (CBETA) fired its first electron beam tests using the first pass (S1) splitter line and first girder of the return loop (FA). At various locations on the S1 Line and FA section, the positions of the electron beam were recorded using ten Beam-Position-Monitors (BPMs) as the strength of the steering and focusing electromagnets were varied. Datasets from these tests contain measurements of beam position during magnet scans for the following beam momenta: $38, 42, 47$, and 53MeV. An additional dataset was taken at the momentum 42MeV again, but this time after turning off the eight quadrupole magnets. Analyzing these datasets, this paper will characterize the steering electromagnets on CBETA's S1 Splitter Line by using a subsection of the data recorded to calculate the magnet's apparent calibration value and compare it to the design value. This subset of the available data, the beam position measurements from the closest-downstream BPM, is furthermore used to measure the relative roll angle between magnet-BPM pairs. After disregarding datasets obstructed by alignment errors (characterizations of magnets MD1DIP01, MS1DIP07, MS1DPB01/08 and MS1CRV04 are inconclusive in this study), we find the calibration accuracy for dipoles and vertical correctors are between $1\% - 9\%$ and $2\% - 3\%$ of their design values respectively. Many apparent dipole calibration values are in agreement with their design value; most measurements for the vertical correctors are as well. Furthermore, we find that our study can determine relative roll angles within uncertainties ranging between $5 - 20$milliradian for dipoles and $8 - 30$milliradian for vertical correctors. In many cases, the roll angle uncertainty is larger than the roll angle measurement; the calculations for these cases are consistent with zero relative roll angle between a magnet-BPM pair. In the other cases where the measured roll angle is larger than the uncertainty, more investigation is needed to make sense of the source.

Introduction

A New York State Energy Research Development Authority grant was awarded jointly to Cornell University and Brookhaven National Laboratory for the production of a multiple-pass, energy-recovering accelerator. Eventually to be augmented at Brookhaven National Laboratory, this project starts with a proof of concept experiment to be built at Cornell University. This project is known as the Cornell-University Brookhaven-National-Laboratory Energy-Recovery-Linac Test Accelerator (CBETA); its goal is to build a four-pass accelerator that can recover energy used to accelerate the electron beam.

The electron beam is accelerated through the Main Linac Cryomodule (MLC), which is comprised of six superconducting radiofrequency cavities. These cavities generate an alternating electric field, that, with the correct in-phase entrance timing, accelerates electron beam as bunches pass through each cavity. CBETA is designed to make four passes through the MLC, each time increasing the beam momenta to $42, 78, 114$, and finally 150MeV. The MLC also allows for energy recovery each time the beam enters the MLC thereafter, exactly out of phase. The trajectory and timing of these passes at four different momenta is handled by the Splitter and Re-Combiner Lines on each side of the MLC (SX and RX respectively). With completion of the return loop and the splitter line underway, CBETA ran initial tests of the first splitter line (S1) and first girder (FA) of the return loop comprised of Fixed Field Alternating-

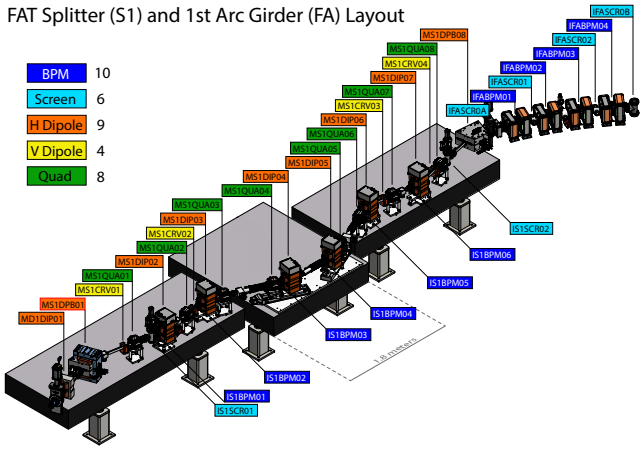

Figure 1. S1 Splitter Line and First Girder Layout [3].

Gradient permanent magnets (FFA). These initial tests are called the Fractional Arc Test (FAT).

The CBETA S1 Splitter Line and FA

The Fractional Arc Test ran a single pass of electrons through the injector, the MLC, the S1 Line, and finally the FA girder (Fig. 1 shows the S1 and FA sections). During the FAT, downstream of the MLC, the electron beam encountered a temporary dipole, D1, which marked the beginning of the S1 Line. When CBETA runs multiple passes once the other splitter lines are commissioned, a Common Dipole (common to all seven passes) will permanently replace the D1 magnet and be used to divide the beams based on their momenta. Once separated, their time of flight and entrance position into the return loop will be finely adjusted. This is designed to ensure proper orbit and timing for re-entry into the MLC. The RX serves a complimentary purpose directly upstream from the MLC.

Beam Position Data Collection

During the FAT, beam position data was taken as magnet strengths were scanned. A total of twenty-one magnets were scanned, consisting of dipole, vertical corrector, and quadrupole magnets. These scan settings were generally based around the nominal current settings for a reference orbit. This paper will analyze the dipole and vertical corrector scans at the beam momenta and conditions: $38, 42, 47, 53$MeV, and 42MeV again with the quadrupole magnets turned off.

Each data set consists of one magnet current setting, readback values for all magnets, ten beam position measurements, and ten pulse height values. The setting value confirmed the excitation current being varied, quoting the readback value of the magnet being scanned in units of Amps. The readback values verify the settings of each magnet of the type being scanned, also in units of Amps. From each of the ten beam-position-monitors (BPMs) at various locations on the S1 Line and FA girder, a horizontal and vertical beam position was recorded in units of millimeters. Additionally, a pulse height value of arbitrary units accompanied each pair of position measurements.

Beam position measurements are made using the currents in four electrodes positioned around the beam pipe at a single location. These four electrodes make up one BPM. The pulse height value for a position measurement is produced by digitalizing the current readings from all four electrodes. In its digital format, these numbers are summed, the final output being a scaled number of arbitrary units. We use these pulse height values to ensure a beam was present for each position measurement. In the event that the beam is steered into the side of the beam-pipe upstream of a BPM, that BPM will produce an arbitrary position measurement that has no physical significance. After identifying arbitrary measurements based on their distinctively low pulse height value, we remove that data from further analysis. For the BPMs on the S1 Line and FA Girder section respectively, we removed measurements with pulse height values below the threshold of $8,000$ and $10,000$. Furthermore, it should be noted that the threshold pulse height for the first BPM of the FA section (IFABPM01) is uniquely $200,000$.

For example, as the excitation current is varied in an upstream magnet, the beam passes through a BPM downstream in multiple locations. In Fig. (2), the beam measurements from several scan settings have pulse height values well below the threshold listed above. This suggests that at those settings, the beam missed the range of the BPM or hit the side of the beam pipe upstream of the BPM. Thus, for this example, we would expunge measurements from the two lowest and the three highest current settings before further analysis.

After removing these low pulse height measurements, we can plot the remaining horizontal and vertical beam position measurements against the scan settings

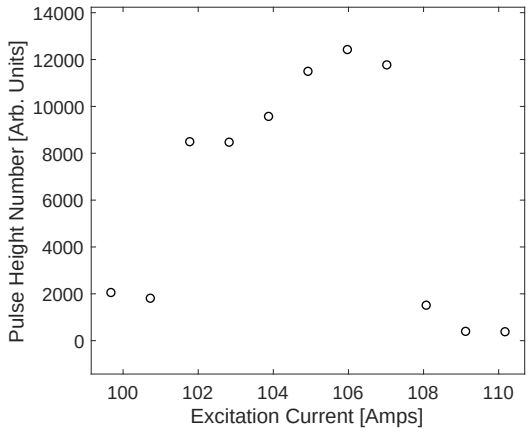

Figure 2. MS1DIP03 scan pulse height values measured at IS1BPM04 from the 42MeV Scan dataset. Measurements with pulse height values below 8000 were removed from dataset.

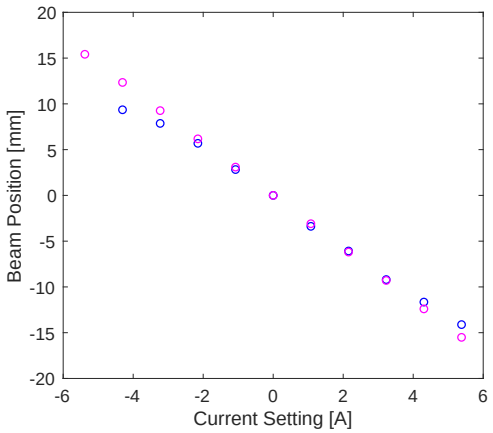

Figure 3. MS1DIP06 scan horizontal beam position measured at IS1BPM06: Virtual Machine replicated data in magenta overlaid with observed data in blue. This data is from the 42MeV Scan dataset.

of a magnet upstream. Fitting a function to these plots, we set out to calculate the linear slopes ($\frac{\Delta x}{\Delta I}$) and ($\frac{\Delta y}{\Delta I}$) for dipoles and vertical correctors respectively. We use these values to assess the accuracy of the virtual machine simulation [3] and to characterize each magnet.

Since dipoles are designed to steer the beam in the horizontal direction only, we expect scans of these magnets to yield nonzero slope from horizontal data and zero slope from vertical data. The reciprocal is true of the vertical correctors. Therefore, to generalize terminology henceforth, I will refer to the direction of expected steering as the design direction in x.

Nonlinearity of the Beam Position Monitors

It is well established that the mechanism used in BPMs is increasingly nonlinear further from the center. These nonlinear effects cause the reported position measurement to be closer to the origin than the beam's physical position. Correction functions are currently used to rectify some of the nonlinear effects [3], however these effects were still visibly noticeable in our datasets, lowering the slope measurement. Seen in Fig. (3), the measured dataset (blue) follows a cubic shape rather than a strictly linear form demonstrated by the virtual machine (magenta). Notice that the datasets agree inside a small range near the origin, but begin to diverge further from the center of the BPM. This behavior is characteristic of BPM nonlinearity, and is therefore not necessarily indicative of physical disagreement between measured and simulated data.

Because this phenomenon is understood to be strictly cubic in nature, we are able to account for the BPM nonlinearity and retrieve the slope value, $\frac{\Delta x}{\Delta I}$, by fitting the measured data to the cubic function:

$$\hat{y} = C_3 x^3 + C_1 x + C_0, \tag{1}$$

where C_3 is the cubic coefficient, C_1 is the linear coefficient (henceforth referred to as the cubic term and linear term respectively), and C_0 is an offset term.

Using this cubic fit in our analysis, the slope $\frac{\Delta x}{\Delta I}$ is simply the linear term, C_1. The offset term, C_0, is included to account for the uncertainty in the measurement of the nominal position, which is subtracted from the raw scan data during analysis. Without this offset parameter, the accuracy of the cubic and linear fit parameters would be sacrificed to ensure the fit function passes through the origin, which is in no way paramount. Notice that there is no quadratic parameter present since the BPM nonlinearity is strictly cubic. Besides the fact that there is no physical purpose to include it, the presence of an superfluous quadratic term would increase the number of fit parameters thereby inappropriately reducing the reported measurement uncertainty.

The presence of C_3 as a fit parameter is of nontrivial rationale. Because we measure the slope from the same BPM for multiple scans, it would supply the same nonlinearity in each measurement. However, the nonlinear

effect is unique to the beam position in the BPM range, and since the nominal position is subtracted from the entire scan prior to cubic fitting, the nonlinear effect is not consistent in each dataset even for the same BPM. This could have been accounted for by finding the relationship between cubic term and position in the BPM range, however another complications arises. For instance, a dipole scan ideally only changes the horizontal position of the beam downstream, however, this is not strictly the case in most measured datasets. We see the beam position scan along a diagonal in most cases, changing in both x and y and thus entering the BPM at different vertical positions. Therefore the cubic term even within a dataset is not consistent. This fact further complicates cubic generalization in any BPM, rendering the exercise of obtaining a characteristic cubic term ineffectual for this study. Currently, a solution to this problem is being implemented for future BPM position measurements [3].

Determining X and Y Accuracy and Slope Variance

To retroactively calculate the uncertainty in position measurement, a quantity eventually used to weight a fit and calculate the sole variance, we used common statistical methods briefly outlined here.

The magnitude of position measurement error bars, s_y, is calculated as follows,

$$s_y^2 = \frac{1}{n-p} \cdot \sum_{i=1}^{n} (y_i - \hat{y}_i)^2 \tag{2}$$

where n is the number of data points, y is a position measurement, $\hat{y}$ is the cubic fit function outlined in the previous section, and p is the number of fit parameters. In our case, we use $p = 3$ (see Eq. 1). Notice that this equation is closely related to χ^2, but with an extra term, which relates the number of data points and fit parameters. Clearly, fitting a function with the same number of parameters as there are data points yields $\chi^2 = 0$. This explains the s_y dependence on the number of data points exceeding the number of parameters.

We use the value of s_y to determine the slope variance in our nonlinear fit as follows,

$$\delta m^2 = \frac{s_y^2}{\sum_{i=1}^{n} (x_i - \bar{x})^2} \tag{3}$$

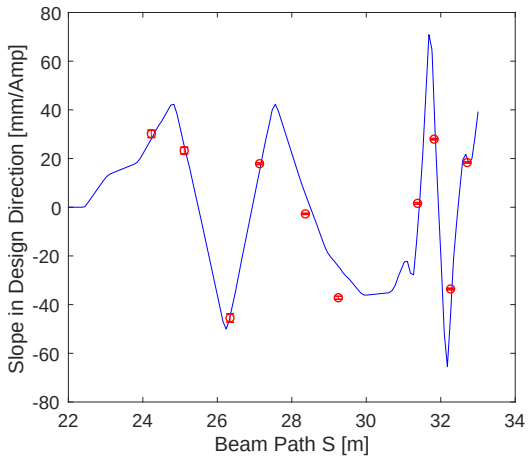

Figure 4. Virtual Machine Continuous Function of Slope overlaid with Horizontal Beam Position from the 42MeV Scan dataset for the magnet MD1DIP01.

where δm is the slope uncertainty, x is the change in excitation current, and $\bar{x}$ is the average value of x. We use the value from Eq. 3 to linearly propagate uncertainty in the calculations that follow.

Virtual Machine Slope Comparison at 42 MeV

After obtaining measurements of the slope, $\frac{\Delta x}{\Delta I}$, and slope uncertainty, δm, we used the following technique to compare measurement and simulation data for the 42MeV Scan dataset. Plotted in Figures (4-16) are continuous functions showing slope values along the virtual beam trajectory (blue), overlaid with the measured slope values from real BPMs (red). The virtual machine allows us to plot a continuous trajectory of slope values by graphing the offset in nominal trajectory for a small change in an element's current, that is the change in position due to a change in current. Dividing that continuous path by the aforementioned change in current yields a continuous function of slope in the units of millimeters per Amp, the same value we calculate in the linear term of the cubic fit.

It is clear from Figures (4-16) that our slope measurement is generally speaking in agreement with the virtual machine's assumed calibration values to the few percent level, however, some discrepancies exist. On the one hand, these discrepancies may be due to the virtual machine's assumed calibration being inaccurate. On the other hand, discrepancies may be due to the physical limitations of the beam pipe dimensions causing the

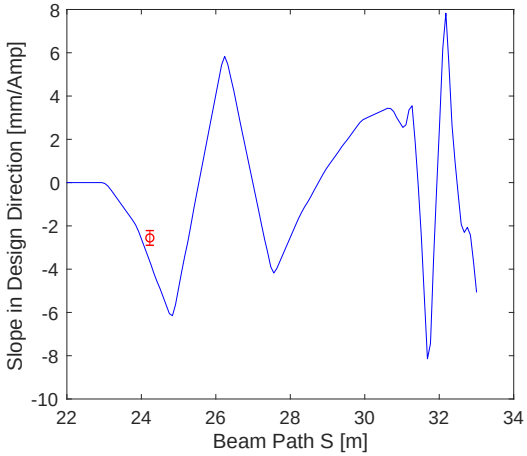

Figure 5. Virtual Machine Continuous Function of Slope overlaid with Horizontal Beam Position from the 42MeV Scan dataset for the magnet MS1DPB01.

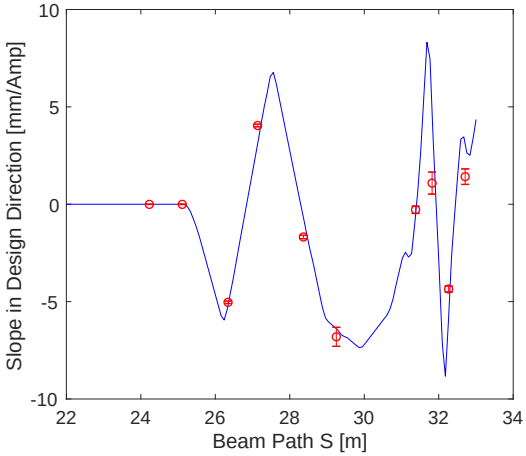

Figure 7. Virtual Machine Continuous Function of Slope overlaid with Horizontal Beam Position from the 42MeV Scan dataset for the magnet MS1DIP03.

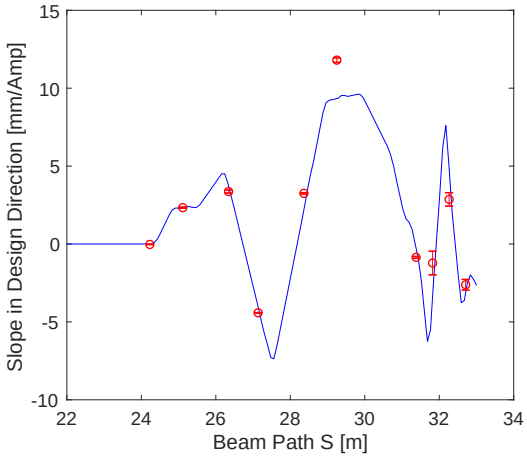

Figure 6. Virtual Machine Continuous Function of Slope overlaid with Horizontal Beam Position from the 42MeV Scan dataset for the magnet MS1DIP02.

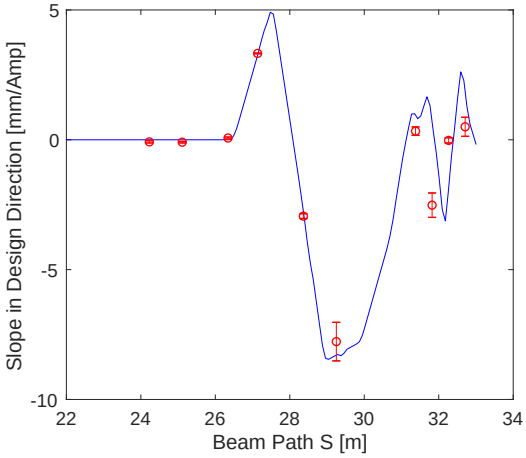

Figure 8. Virtual Machine Continuous Function of Slope overlaid with Horizontal Beam Position from the 42MeV Scan dataset for the magnet MS1DIP04.

slope measurements to be inaccurate. The beam pipe has a physical height of 24mm and a width of 36mm. Consequently, the further the beam is steered away from the nominal trajectory and closer to the walls, the fewer data points are probably available to the BPM. This may present an issue in slope measurement accuracy for beam steered far from its nominal trajectory since, due to the nonlinearity phenomenon, ideally data points should be available both further away and closer to zero. To be included in the slope measurements, BPM data sets need a minimum of four data points. This is because our nonlinear fit (Eq. 1) has three parameters, and an additional data point on top of that amount is needed to produce a measurement uncertainty. BPM data sets with fewer than four non-arbitrary points were omitted from these plots (Fig. 4-16), which goes to explain the absence of slope measurements on some plots (namely in Fig. 5).

Magnet Characterization Tables

Magnets on the S1 Splitter Line were characterized as follows: horizontal and vertical bend angle at nominal current in units of radians, change in horizontal and

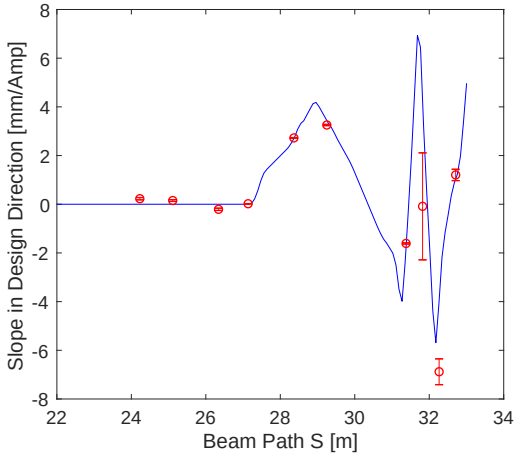

Figure 9. Virtual Machine Continuous Function of Slope overlaid with Horizontal Beam Position from the 42MeV Scan dataset for the magnet MS1DIP05.

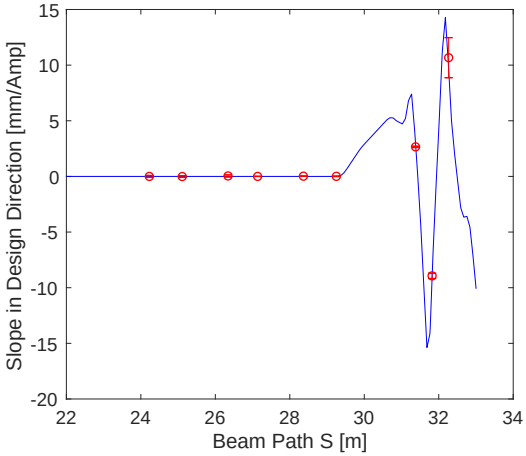

Figure 11. Virtual Machine Continuous Function of Slope overlaid with Horizontal Beam Position from the 42MeV Scan dataset for the magnet MS1DIP07.

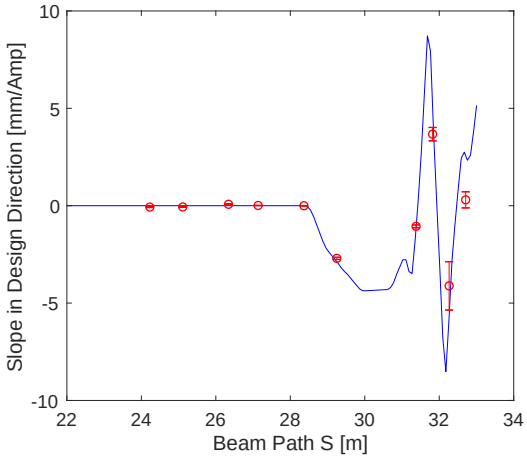

Figure 10. Virtual Machine Continuous Function of Slope overlaid with Horizontal Beam Position from the 42MeV Scan dataset for the magnet MS1DIP06.

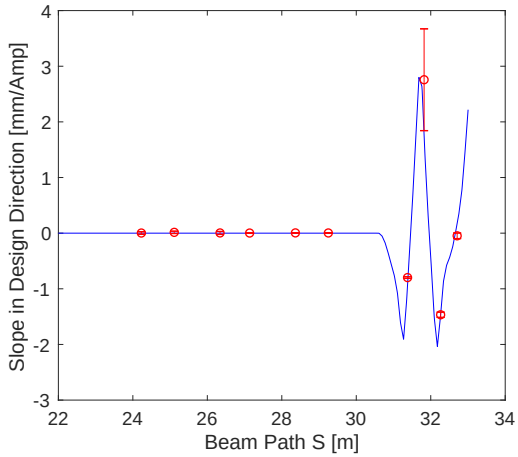

Figure 12. Virtual Machine Continuous Function of Slope overlaid with Horizontal Beam Position from the 42MeV Scan dataset for the magnet MS1DPB08.

vertical bend angle per change in current in units of radians per Ampere, calibration value in units of Tesla meters per Ampere, and roll angle in units of radians. These tables themselves can be found in Appendix A and B, while the discussion of their calculation and values will follow.

Calculation of the Values in the Characterization Tables

It is well known in the field of accelerator physics that the position and angle of a particle beam at some point depend linearly on that beam's initial position and angle at some earlier point upstream. In principle, this is because the direction of the kick supplied is always a function of entrance position in that direction. That is to say for example, a kick in the x direction is a function of x entrance position and is therefore decoupled from entrance position in the orthogonal direction. This is true for all the magnet elements used to steer or focus the beam (dipole, vertical corrector, and quadrupole magnets). By this design, the linear system can be conveyed

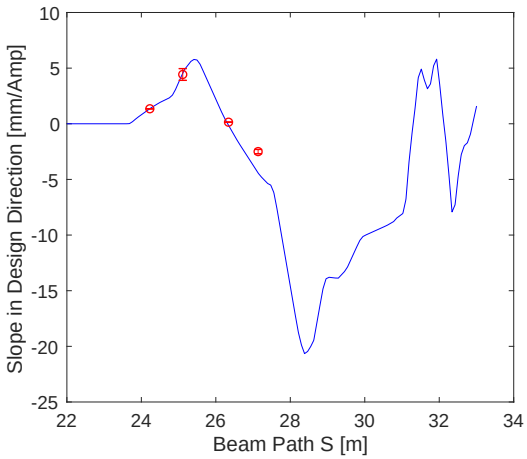

Figure 13. Virtual Machine Continuous Function of Slope overlaid with Vertical Beam Position from the 42MeV Scan dataset for the magnet MS1CRV01.

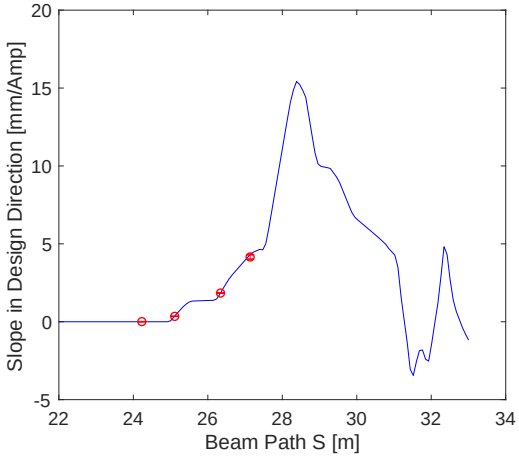

Figure 14. Virtual Machine Continuous Function of Slope overlaid with Vertical Beam Position from the 42MeV Scan dataset for the magnet MS1CRV02.

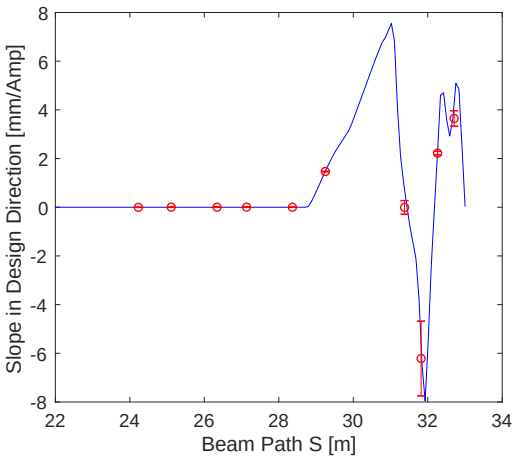

Figure 15. Virtual Machine Continuous Function of Slope overlaid with Vertical Beam Position from the 42MeV Scan dataset for the magnet MS1CRV03.

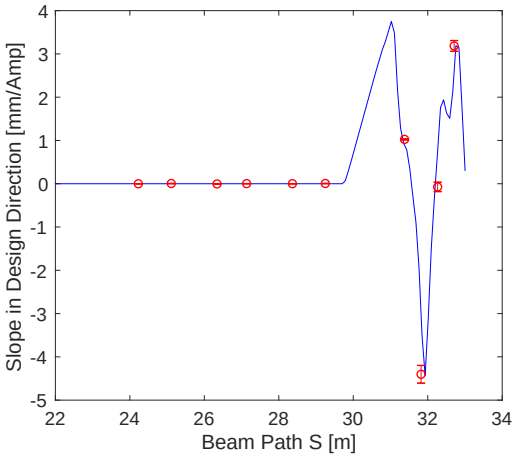

Figure 16. Virtual Machine Continuous Function of Slope overlaid with Vertical Beam Position from the 42MeV Scan dataset for the magnet MS1CRV04.

in transfer matrix formalization:

$$\begin{bmatrix} x \\ x' \end{bmatrix} = \begin{bmatrix} M_{11} & M_{12} \\ M_{21} & M_{22} \end{bmatrix} \begin{bmatrix} x_o \\ x'_o \end{bmatrix}, \tag{4}$$

where x is the final beam position, x' is the final beam angle (here, prime notes the derivative with respect to beam path), x_o is the beam entrance position, x'_o is the beam entrance angle, and the 2×2 matrix is the transfer matrix. It follows from this general equation that between any two points along the beam trajectory, there exists a transfer matrix, the terms of which depend on the intermediate elements. For the specific dataset of this study, the most significant relationship is between the beam entrance angle and the final beam position at a downstream BPM. Because the beam entrance angle depends on the magnet strength, which is varied by excitation current, we can find the equation:

$$\frac{\Delta\theta}{\Delta I} = \frac{\Delta x}{\Delta I} \cdot \frac{1}{M_{12}} = \frac{C_1}{M_{12}}. \tag{5}$$

This expression is executed by consulting the virtual machine for an M_{12} term since the virtual machine's simulation of beam trajectory is entirely based on transfer matrices. In Appendices A and B, this expression is

used to calculate bend angle per current and bend angle at nominal current, both in the direction perpendicular to design; that is the vertical direction for dipoles and the horizontal direction for vertical correctors. This is done only for the direction perpendicular to design because there is a more robust alternative for analysis in the direction of design.

This alternative approach relies on the virtual machine to account for the dynamic nature of the transfer matrix as a magnet is scanned. The improvement is subtle, but more suitable for the reasoning that follows. To properly use a transfer matrix, in this study, we chose two points to begin and end a path segment for which the transfer matrix is calculated. The path segment is from the center of the scanning magnet to the nearest BPM downstream. Using the same transfer matrix for multiple excitation currents is problematic because, for different current settings, the transfer matrix is evidently different since the beam is recorded off of its nominal trajectory downstream. Therefore, with this enhanced method, we use the virtual machine to plot a pilot point that demonstrates the change in the transfer matrix rather than calculating it only once.

To plot a pilot point in the virtual machine from each magnet to the closest-downstream BPM, first we directly changed the magnetic field in a magnet, thereby bypassing the virtual machine's assumed proportionality between current and magnetic field, one of the values we seek to measure. Next, we recorded the change in virtual beam position at the real position of the first BPM downstream. This gives us the value for K_{vm}, where

$$K_{vm} = \frac{\Delta x_{vm}}{\Delta B_{vm} L}. \tag{6}$$

The subscript *vm* reminds us that these quantities are set or recorded in the virtual machine. The measured dataset produces its own $K_{measured}$ value, which, when set equal to that of the virtual machine, yields the following equation for calibration value:

$$\int \alpha \cdot dl = \frac{(\frac{\Delta x}{\Delta I})_{measured}}{K_{vm}}. \tag{7}$$

This calibration value, along with beam momentum of each dataset, is furthermore used to calculate bend angle per current and bend angle at nominal current, both in the direction of design. All three of these values are in Characterization Tables found in Appendices A and B. Note that this dynamic approach to the transfer matrix could not have been implemented in the direction perpendicular to design because the virtual beam position in this direction is intentionally zero.

Lastly, we can calculate the roll angle between a magnet and its closest downstream BPM. This is not an absolute roll angle because absolute roll angle of either element would be indiscernible by these methods of analysis. Therefore, we can only make statements about the roll angle of an element with respect to another element. This relative roll angle is calculated by the expression: $\frac{\Delta y}{\Delta x} \cdot \frac{\pi}{4}$, where x is the designed kick direction, and y is perpendicular to x. We determined the uncertainty in all measurements using linear propagation of uncertainty.

Calibration Value of the Magnets on the S1 Splitter Line

In August of 2017, Bass reported on the design of the dipoles characterized in this paper. Design values from her report are displayed as the Expected Field Integral Along the Trajectory found in the Characterization Tables (Appendix A and B) [2]. In the context of this study, those numbers are used to compare the measured data from FAT with the that of the virtual machine simulation, which uses a lattice of ideal design values and zero roll angle. With that in mind, the calibration values of the dipole magnets generally seem to be accurate to their expected field integral within $1\% - 9\%$ accuracy for four datasets (the dataset 42 MeV Quadrupoles Off is omitted from these results for reasons expounded upon in a subsequent section). We find that the spread of apparent calibration values is usually above or below the expected value. Rarely do we see the spread in calibration values to be exactly centered around the expected value. This points us away from the idea that these small discrepancies are random error and suggests discrepancy is something systematic.

Furthermore, on most of these highly accurate calculations, the reported 1σ uncertainty is often in agreement with the expected value, although this is not true for several calculations. The reported 1σ uncertainty varies over the range from 5 to 20 micro-Tesla meters per Amp. For calculations with relatively small uncertainties, the expected value is often a few σ away and therefore not in strict agreement.

For the vertical correctors, the calculations are generally accurate within $2\% - 3\%$ of the expected calibration value. These calculations also show low uncertainties ranging around $1.5 - 3.5$ micro-Tesla meters per Amp. For calculations with these uncertainties, the expected value is up to 2σ away, and thus not in strict agreement.

Roll Angle Sensitivity in Data Analysis for Magnets on the S1 Splitter Line

For the roll angle measurements in the Characterization Tables, we see low spread in the calculated values. Here we do not compare the data to the virtual machine since the roll angle is a measurement of an imperfection of magnet commissioning or installation. While our measurements of relative roll angle are generally within the range of tens of milliradian, the value of significance is our sensitivity to roll angle measurement. Generally, but varying over different datasets, our sensitivity to roll angle is around $5 - 20$milliradian and $8 - 30$milliradian for dipoles and vertical correctors respectively. While this sensitivity is reasonably high, commissioning professionals have a significantly lower roll-angle measurement uncertainty, close to a few milliradian. Therefore our measurements of roll angle are probably not components of an absolute roll, but indicators of intermediate magnet roll angle as well. However, this study lacks data to confirm this definitively.

Datasets and Tables of Inconclusive Analysis

The dataset 42MeV Quadrupoles Off is omitted from the reported results of the preceding two sections because, for this dataset, our analysis is left inconclusive. This dataset consistently produced outlying measurements because the beam was steered far from the nominal trajectory in both the vertical and horizontal directions making the K_{vm} inapplicable to this dataset. This large-scale steering is due to the nominal trajectory being steered by quadrupole magnets as a result of entering their magnetic field off-axis, a benign condition recognized by operators of the FAT at the time. However, in absence of this quadrupole steering, our analysis of this dataset is unsuitable. This statement is corroborated by the fact that the 42MeV Quadrupoles Off dataset yields the most consistently inaccurate measurements. Because we are aware of the reason for these deviations, the measurements are omitted from our reported results.

Additionally, our analysis of magnets: MD1DIP01, MS1DIP07, MS1CRV04, and the sector magnets MS1DPB01/08, is inconclusive across datasets. These magnets all have an intermediate sector magnet between their position and their closest-downstream BPM or are the sector magnets themselves.

The reason our analysis is inconclusive for data traversing sector magnets has to do with their high level of sensitivity to entrance position. Again, inconclusive analysis can be corroborated by the fact that data for these magnets are in large disagreement with expected values and have quite a large spread between datasets. Because the reported uncertainty is approximately in the same range as other magnets, it is clear that the error is not necessarily in the slope calculation, but rather the calculation utilizing K_{vm} or M_{12}. This complication will be expounded upon in the following sections.

Dataset Conditions and Their Significance

During the FAT, beam momentum was known to an estimated 1% uncertainty. It should be noted that currently, analysis is being done on the MLC to obtain finer quantitative values for the uncertainty in beam momentum, uncertainty in entrance position into the S1 line, and other factors beyond the scope of this paper [3]. Since this analysis is on-going, no uncertainty is displayed in the Characterization Tables for the value for Expected Field Integral Along Trajectory despite the call for one. Even while the to-date uncertainty estimation propagates into every single calculation made in this study, it's maximum effect on our calculations is no more than a couple percent.

However, the factor that causes significantly higher error is the large deviations in entrance position into the S1 Line between datasets. Figures 17 and 18 show a plot of nominal beam trajectories for multiple data sets. Each vertical black line shows the position of a BPM, and the red stars indicate a position measurement. The color-coded lines connect the measurements of each dataset.

Interestingly, the trajectories in Figures 17 and 18 are not the same although they all share the same settings that were scaled linearly with beam momentum (and thus should provide the same nominal bend angle). Since in the first BPM they are already not in the same location, this study cannot comment on whether the nominal settings were scaled correctly since the tra-

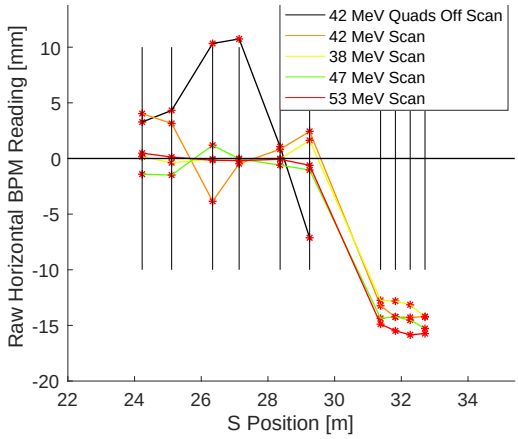

Figure 17. Overlay of Raw Horizontal Beam Position Measurements from Multiple Datasets All at Nominal Settings

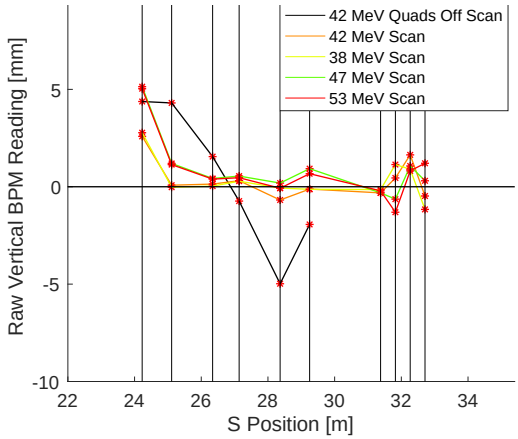

Figure 18. Overlay of Raw Vertical Beam Position Measurements from Multiple Datasets All at Nominal Settings

jectory would be different given these unique entrance positions. Regardless, because the nominal trajectories vary for different datasets, much of the underlying assumptions made in order to calculate the same values are called into question. This entrance error between datasets is very significant to our calculations because it means that both the static M_{12} and dynamic transfer matrix methods are not scalable between datasets depending on the severity of the entrance position error. It is unclear whether or not the entrance error was significant enough to impede our calculations since we measure slopes for calculations, which may or may not be affected. More analysis is required to conclude how these specific deviations of entrance position would affect our calculations and if so, by how much and in what way.

Discrepancies Discussion and Measured and Simulated Data Comparison

Because the extent of the effects of entrance position errors is not fully known, to clearly see the comparison of the FAT data and simulation, the most prudent comparison is not through Characterization Tables but through inspection of the slope values of each data set (see Figures 4-16). This is because the Characterization Tables use a K_{vm} value, which adds discrepancy between the measured and simulated data, since there are apparently large entrance position errors across measured datasets. In contrast, the continuous function of slope and slope measurements do not appear to use assumptions undermined by entrance position errors.

Furthermore, the error in K_{vm} due to entrance position variation is especially sensitive to calculations traversing intermediate sector magnets (MS1DPB01/08), the field integral of which varies based on entrance position due to geometry of the magnet. This explains why Characterization Table values for magnets MD1DIP01, MS1DIP07, MS1CRV04, and the sector magnets themselves are so inaccurate. Varying nominal trajectories between datasets at different energies means K_{vm} values apparently do not linearly scale with beam energy as supposed. For the sector magnets, this presents a large problem and is why we are see such discrepancy with data that involves sector magnets. Furthermore, erroneous entrance position between datasets impairs all measurements from IFABPM01. Because this BPM is positioned in the FFA, among permanent magnets which cannot scale with energy, erroneous entrance positions that are not correlated with beam energy leave the data in the FFA useless.

Direction for Future Investigation

At the present moment, a better correction function is being implemented for future use in the BPMs [3]. This means their nonlinear effects will be subdued making slope measurements easier and more certain in the future.

For the magnets and datasets of inconclusive analyses, new data should be taken but this time eliminat-

ing the varying, erroneous entrance positions between datasets. Entrance position should be much more consistent and carefully monitored. Additionally, to eliminate a potentially large roll angle factor, and also to make use of the Quadrupoles Off dataset, the beam at nominal trajectory should be steered through the center of the quadrupole magnets to simplify beam steering for analysis. Since this was not the case in the FAT, it is still unclear the actual source of calculated roll angle in this study. A current hypothesis is that roll angles seem to measure intermediate quadrupole roll angles. Steering through the center of the quadrupole magnets would eliminate this. However, more analysis should be done using quadrupole scans to assess the validity of this hypothesis.

Conclusion

With the FAT data, we were able to characterize the dipoles and vertical correctors on the CBETA's S1 Splitter Line. This study is found to have inconclusive data on magnets MD1DIP01, MS1DIP07, MS1DPB01/08 and MS1CRV04. This study reports that the calibration values of the remaining dipoles are within $1\% - 9\%$ of their design values. The remaining S1 vertical correctors are within $2\% - 3\%$ of their design values. For dipoles and vertical correctors respectively, the strongest calculated roll angle sensitivity was 5milliradian and 20milliradian respectively. These sensitivities are below that of the installation survey. Despite this roll angle sensitivity, our measurements often show a nonzero relative roll angle, however, more data and analysis is needed to understand the source of the roll angle calculations specifically.

Acknowledgements

I would first like to acknowledge and thank Jim Crittenden for his role as my mentor. His contributions include data taking, directional instruction, discussion, and editing. Thanks to Colwyn Gulliford for his Correction Function in addition to his advice and support. Thanks to Adam Bartnik for his coding support and advice. Finally, I would also like to acknowledge the generosity and support of the Cornell Laboratory for Accelerator-Based Sciences and Education and the National Science Foundation's award PHY-1757811 for the REU Site Accelerator Physics and Synchrotron Radiation Science at Cornell University, making this research possible.

References

[1] Morrison A. F., "Obtaining Uncertainty Measurements on Slope and Intercept of a Least Squares Fit with Excel's LINEST," Michigan Technical University, (5-6), (2014).

[2] Bass, R., "Comprehensive Tracking Study for the H-Dipoles and Common Magnets in the Splitter Sections of the Cornell/Brookhaven Energy-Recovery-Linac Test Accelerator", CLASSE, (2017).

[3] Gulliford, C., et al. "Beam Commissioning Results from the CBETA Fractional Arc Test" [Internal Document at Cornell in Preparation for Publication] (3-10), (2018).

Appendix A: S1 Dipole Characterization Tables

	Bend angle (horizontal) at Nominal Current [Radians]	Bend angle (vertical) at Nominal Current [Radians]	Horizontal Bend Angle / Current [Radians/Amp]	Vertical Bend Angle / Current [Radians/Amp]	Calibration Value [Tesla Meters/Amp]	Expected Field Integral Along Trajectory [Tesla Meters/Amp]	Roll Angle [Radians]
42MeV Quads Off	2.74e-02 ± 1.4e-03	-3.47e-03 ± 4.4e-04	1.602e-02 ± 8.1e-04	-2.03e-03 ± 2.6e-04	2.24e-03 ± 1.1e-04	3.05e-03	-1.99e-01 ± -2.7e-02
42MeV Scan	4.00e-02 ± 2.0e-03	-2.66e-03 ± 4.5e-04	2.33e-02 ± 1.2e-03	-1.55e-03 ± 2.6e-04	3.27e-03 ± 1.7e-04	3.05e-03	-1.04e-01 ± -1.8e-02
38MeV Scan	3.017e-02 ± 3.7e-04	-6.7e-04 ± 4.0e-04	1.921e-02 ± 2.4e-04	-4.3e-04 ± 2.5e-04	2.433e-03 ± 3.0e-05	3.05e-03	-3.5e-02 ± -2.1e-02
47MeV Scan	3.243e-02 ± 5.2e-04	-1.18e-03 ± 4.6e-04	1.691e-02 ± 2.7e-04	-6.1e-04 ± 2.4e-04	2.650e-03 ± 4.2e-05	3.05e-03	-5.7e-02 ± -2.3e-02
53MeV Scan	3.338e-02 ± 6.6e-04	-2.2e-04 ± 5.3e-04	1.544e-02 ± 3.1e-04	-1.0e-04 ± 2.5e-04	2.728e-03 ± 5.4e-05	3.05e-03	-1.1e-02 ± -2.5e-02

Table 1

Characterization Table of MD1DIP01 at IS1BPM01

	Bend angle (horizontal) at Nominal Current [Radians]	Bend angle (vertical) at Nominal Current [Radians]	Horizontal Bend Angle / Current [Radians/Amp]	Vertical Bend Angle / Current [Radians/Amp]	Calibration Value [Tesla Meters/Amp]	Expected Field Integral Along Trajectory [Tesla Meters/Amp]	Roll Angle [Radians]
42MeV Quads Off	-5.25e-01 ± 2.8e-02	6.3e-02 ± 3.2e-02	-2.41e-03 ± 1.3e-04	2.9e-04 ± 1.5e-04	-3.38e-04 ± 1.8e-05	3.55e-04	-1.89e-01 ± -9.7e-02
42MeV Scan	-3.87e-01 ± 5.2e-02	6.6e-02 ± 4.9e-02	-1.78e-03 ± 2.4e-04	3.0e-04 ± 2.3e-04	-2.49e-04 ± 3.3e-05	3.55e-04	-2.7e-01 ± -2.1e-01
38MeV Scan	-5.29e-01 ± 1.3e-02	3.0e-02 ± 4.7e-02	-2.654e-03 ± 6.7e-05	1.5e-04 ± 2.3e-04	-3.361e-04 ± 8.5e-06	3.55e-04	-9.e-02 ± -1.4e-01
47MeV Scan	-6.0407e-01 ± 2.0e-04	-1.2e-02 ± 4.8e-02	-2.45996e-03 ± 8.3e-07	-5.e-05 ± 2.0e-04	-3.8539e-04 ± 1.3e-07	3.55e-04	3.e-02 ± 1.3e-01
53MeV Scan	-5.30e-01 ± 1.7e-02	-1.1e-02 ± 2.2e-02	-1.905e-03 ± 6.0e-05	-4.0e-05 ± 8.0e-05	-3.37e-04 ± 1.1e-05	3.55e-04	3.4e-02 ± 6.8e-02

Table 2

Characterization Table of MS1DPB01 at IS1BPM01

	Bend angle (horizontal) at Nominal Current [Radians]	Bend angle (vertical) at Nominal Current [Radians]	Horizontal Bend Angle / Current [Radians/Amp]	Vertical Bend Angle / Current [Radians/Amp]	Calibration Value [Tesla Meters/Amp]	Expected Field Integral Along Trajectory [Tesla Meters/Amp]	Roll Angle [Radians]
42MeV Quads Off	3.153e-01 ± 6.0e-03	-5.86e-02 ± 6.9e-03	5.31e-03 ± 1.0e-04	-9.9e-04 ± 1.2e-04	7.43e-04 ± 1.4e-05	6.98e-04	-2.92e-01 ± -3.5e-02
42MeV Scan	2.975e-01 ± 4.7e-03	-4.3e-03 ± 1.4e-03	5.009e-03 ± 8.0e-05	-7.3e-05 ± 2.3e-05	7.01e-04 ± 1.1e-05	6.98e-04	-2.31e-02 ± -7.3e-03
38MeV Scan	2.966e-01 ± 4.0e-03	-4.0e-03 ± 1.7e-03	5.535e-03 ± 7.4e-05	-7.6e-05 ± 3.2e-05	7.011e-04 ± 9.4e-06	6.98e-04	-2.16e-02 ± -9.2e-03
47MeV Scan	2.922e-01 ± 1.9e-03	-4.9e-03 ± 1.4e-03	4.433e-03 ± 2.9e-05	-7.5e-05 ± 2.1e-05	6.946e-04 ± 4.5e-06	6.98e-04	-2.67e-02 ± -7.5e-03
53MeV Scan	3.041e-01 ± 4.2e-03	-3.2e-03 ± 1.2e-03	4.067e-03 ± 5.6e-05	-4.2e-05 ± 1.6e-05	7.185e-04 ± 9.9e-06	6.98e-04	-1.65e-02 ± -6.2e-03

Table 3

Characterization Table of MS1DIP02 at IS1BPM02

	Bend angle (horizontal) at Nominal Current [Radians]	Bend angle (vertical) at Nominal Current [Radians]	Horizontal Bend Angle / Current [Radians/Amp]	Vertical Bend Angle / Current [Radians/Amp]	Calibration Value [Tesla Meters/Amp]	Expected Field Integral Along Trajectory [Tesla Meters/Amp]	Roll Angle [Radians]
42MeV Quads Off	-3.23e-01 ± 2.1e-02	3.57e-02 ± 8.6e-03	-3.07e-03 ± 2.0e-04	3.40e-04 ± 8.2e-05	-4.30e-04 ± 2.8e-05	6.98e-04	-1.74e-01 ± -4.3e-02
42MeV Scan	-5.078e-01 ± 6.3e-03	-4.6e-03 ± 3.2e-03	-4.840e-03 ± 6.0e-05	-4.3e-05 ± 3.0e-05	-6.776e-04 ± 8.4e-06	6.98e-04	1.43e-02 ± 1.0e-02
38MeV Scan	-5.10e-01 ± 1.5e-02	1.9e-03 ± 1.8e-03	-5.36e-03 ± 1.5e-04	2.0e-05 ± 1.9e-05	-6.79e-04 ± 2.0e-05	6.98e-04	-6.0e-03 ± -5.5e-03
47MeV Scan	-5.31e-01 ± 1.2e-02	1.01e-03 ± 9.0e-04	-4.52e-03 ± 1.0e-04	8.6e-06 ± 7.7e-06	-7.08e-04 ± 1.6e-05	6.98e-04	-3.0e-03 ± -2.7e-03
53MeV Scan	-4.67e-01 ± 1.4e-02	5.e-04 ± 1.4e-03	-3.49e-03 ± 1.1e-04	4.e-06 ± 1.0e-05	-6.16e-04 ± 1.9e-05	6.98e-04	-1.8e-03 ± -4.7e-03

Table 4

Characterization Table of MS1DIP03 at IS1BPM03

	Bend angle (horizontal) at Nominal Current [Radians]	Bend angle (vertical) at Nominal Current [Radians]	Horizontal Bend Angle / Current [Radians/Amp]	Vertical Bend Angle / Current [Radians/Amp]	Calibration Value [Tesla Meters/Amp]	Expected Field Integral Along Trajectory [Tesla Meters/Amp]	Roll Angle [Radians]
42MeV Quads Off	NA	NA	NA	NA	NA	6.98e-04	NA
42MeV Scan	3.961e-01 ± 1.7e-03	2.4e-03 ± 2.4e-03	5.078e-03 ± 2.2e-05	3.1e-05 ± 3.0e-05	7.110e-04 ± 3.1e-06	6.98e-04	9.8e-03 ± 9.4e-03
38MeV Scan	3.933e-01 ± 3.2e-03	2.2e-03 ± 1.6e-03	5.528e-03 ± 4.5e-05	3.1e-05 ± 2.3e-05	7.002e-04 ± 5.7e-06	6.98e-04	8.7e-03 ± 6.5e-03
47MeV Scan	3.847e-01 ± 3.3e-03	2.6e-03 ± 4.1e-03	4.381e-03 ± 3.7e-05	2.9e-05 ± 4.7e-05	6.864e-04 ± 5.8e-06	6.98e-04	1.1e-02 ± 1.7e-02
53MeV Scan	3.769e-01 ± 2.3e-03	4.1e-03 ± 2.8e-03	3.781e-03 ± 2.3e-05	4.1e-05 ± 2.8e-05	6.680e-04 ± 4.0e-06	6.98e-04	1.7e-02 ± 1.2e-02

Table 5

Characterization Table of MS1DIP04 at IS1BPM04

	Bend angle (horizontal) at Nominal Current [Radians]	Bend angle (vertical) at Nominal Current [Radians]	Horizontal Bend Angle / Current [Radians/Amp]	Vertical Bend Angle / Current [Radians/Amp]	Calibration Value [Tesla Meters/Amp]	Expected Field Integral Along Trajectory [Tesla Meters/Amp]	Roll Angle [Radians]
42MeV Quads Off	4.802e-01 ± 4.5e-03	1.7e-02 ± 3.5e-02	6.110e-03 ± 5.7e-05	2.2e-04 ± 4.4e-04	8.554e-04 ± 8.0e-06	6.98e-04	6.e-02 ± 1.1e-01
42MeV Scan	3.939e-01 ± 2.2e-03	-1.3e-03 ± 4.0e-03	5.012e-03 ± 2.8e-05	-1.7e-05 ± 5.1e-05	7.017e-04 ± 3.9e-06	6.98e-04	-5.e-03 ± -1.6e-02
38MeV Scan	3.898e-01 ± 2.8e-03	-1.2e-03 ± 1.3e-03	5.410e-03 ± 3.9e-05	-1.6e-05 ± 1.8e-05	6.853e-04 ± 4.9e-06	6.98e-04	-4.8e-03 ± -5.4e-03
47MeV Scan	4.288e-01 ± 2.2e-03	-2.5e-03 ± 2.0e-03	4.835e-03 ± 2.5e-05	-2.9e-05 ± 2.2e-05	7.574e-04 ± 3.9e-06	6.98e-04	-9.3e-03 ± -7.2e-03
53MeV Scan	4.357e-01 ± 2.3e-03	-3.2e-03 ± 1.3e-03	4.323e-03 ± 2.3e-05	-3.1e-05 ± 1.3e-05	7.638e-04 ± 4.0e-06	6.98e-04	-1.15e-02 ± -4.7e-03

Table 6

Characterization Table of MS1DIP05 at IS1BPM05

	Bend angle (horizontal) at Nominal Current [Radians]	Bend angle (vertical) at Nominal Current [Radians]	Horizontal Bend Angle / Current [Radians/Amp]	Vertical Bend Angle / Current [Radians/Amp]	Calibration Value [Tesla Meters/Amp]	Expected Field Integral Along Trajectory [Tesla Meters/Amp]	Roll Angle [Radians]
42MeV Quads Off	-5.27e-01 ± 1.6e-02	6.2e-02 ± 1.0e-02	-4.90e-03 ± 1.5e-04	5.76e-04 ± 9.4e-05	-6.86e-04 ± 2.1e-05	6.98e-04	-1.85e-01 ± -3.1e-02
42MeV Scan	-5.04e-01 ± 1.0e-02	-1.21e-02 ± 9.5e-03	-4.680e-03 ± 9.8e-05	-1.12e-04 ± 8.8e-05	-6.55e-04 ± 1.4e-05	6.98e-04	3.8e-02 ± 3.0e-02
38MeV Scan	-5.52e-01 ± 1.5e-02	-1.34e-02 ± 5.9e-03	-5.64e-03 ± 1.5e-04	-1.36e-04 ± 6.1e-05	-7.15e-04 ± 1.9e-05	6.98e-04	3.8e-02 ± 1.7e-02
47MeV Scan	-4.860e-01 ± 1.3e-03	-3.9e-03 ± 4.8e-03	-4.015e-03 ± 1.1e-05	-3.2e-05 ± 3.9e-05	-6.290e-04 ± 1.7e-06	6.98e-04	1.3e-02 ± 1.6e-02
53MeV Scan	-4.552e-01 ± 2.0e-03	-4.2e-03 ± 5.5e-03	-3.292e-03 ± 1.4e-05	-3.0e-05 ± 4.0e-05	-5.816e-04 ± 2.5e-06	6.98e-04	1.5e-02 ± 1.9e-02

Table 7

Characterization Table of MS1DIP06 at IS1BPM06

	Bend angle (horizontal) at Nominal Current [Radians]	Bend angle (vertical) at Nominal Current [Radians]	Horizontal Bend Angle / Current [Radians/Amp]	Vertical Bend Angle / Current [Radians/Amp]	Calibration Value [Tesla Meters/Amp]	Expected Field Integral Along Trajectory [Tesla Meters/Amp]	Roll Angle [Radians]
42MeV Quads Off	NA	NA	NA	NA	NA	6.98e-04	NA
42MeV Scan	3.177e-01 ± 6.9e-03	-9.e-03 ± 1.4e-02	4.60e-03 ± 1.0e-04	-1.3e-04 ± 2.1e-04	6.43e-04 ± 1.4e-05	6.98e-04	-4.6e-02 ± -7.1e-02
38MeV Scan	2.40e-01 ± 1.1e-02	-1.11e-02 ± 5.1e-03	3.79e-03 ± 1.7e-04	-1.75e-04 ± 8.0e-05	4.79e-04 ± 2.1e-05	6.98e-04	-7.3e-02 ± -3.3e-02
47MeV Scan	4.29e-01 ± 1.1e-02	-1.3e-02 ± 1.2e-02	5.53e-03 ± 1.4e-04	-1.6e-04 ± 1.5e-04	8.66e-04 ± 2.2e-05	6.98e-04	-4.6e-02 ± -4.4e-02
53MeV Scan	4.611e-01 ± 7.0e-03	-2.51e-02 ± 5.4e-03	5.228e-03 ± 7.9e-05	-2.85e-04 ± 6.2e-05	9.24e-04 ± 1.4e-05	6.98e-04	-8.5e-02 ± -1.8e-02

Table 8

Characterization Table of MS1DIP07 at IFABPM01

	Bend angle (horizontal) at Nominal Current [Radians]	Bend angle (vertical) at Nominal Current [Radians]	Horizontal Bend Angle / Current [Radians/Amp]	Vertical Bend Angle / Current [Radians/Amp]	Calibration Value [Tesla Meters/Amp]	Expected Field Integral Along Trajectory [Tesla Meters/Amp]	Roll Angle [Radians]
42MeV Quads Off	NA	NA	NA	NA	NA	3.55e-04	NA
42MeV Scan	-4.571e-01 ± 8.4e-03	-1.4e-03 ± 7.0e-03	-2.210e-03 ± 4.1e-05	-7.e-06 ± 3.4e-05	-3.094e-04 ± 5.7e-06	3.55e-04	5.e-03 ± 2.5e-02
38MeV Scan	-4.87e-01 ± 1.3e-02	-6.e-03 ± 1.3e-02	-2.572e-03 ± 6.9e-05	-3.2e-05 ± 7.1e-05	-3.257e-04 ± 8.7e-06	3.55e-04	2.0e-02 ± 4.4e-02
47MeV Scan	-5.567e-01 ± 3.8e-03	3.0e-02 ± 2.0e-02	-2.368e-03 ± 1.6e-05	1.26e-04 ± 8.5e-05	-3.710e-04 ± 2.6e-06	3.55e-04	-8.6e-02 ± -5.8e-02
53MeV Scan	-6.470e-01 ± 5.3e-03	2.1e-02 ± 1.6e-02	-2.415e-03 ± 2.0e-05	7.8e-05 ± 6.1e-05	-4.267e-04 ± 3.5e-06	3.55e-04	-5.2e-02 ± -4.1e-02

Table 9

Characterization Table of MS1DPB08 at IFABPM01

Appendix B: S1 Vertical Corrector Characterization Tables

Notice that the nominal current for the vertical correctors is zero, except for MS1CRV02, which had a nominal current of 1.6306 Amps. Thus, for the other vertical correctors, the first two columns are left blank intentionally.

	Bend angle (horizontal) at Nominal Current [Radians]	Bend angle (vertical) at Nominal Current [Radians]	Horizontal Bend Angle / Current [Radians/Amp]	Vertical Bend Angle / Current [Radians/Amp]	Calibration Value [Tesla Meters/Amp]	Expected Field Integral Along Trajectory [Tesla Meters/Amp]	Roll Angle [Radians]
42MeV Quads Off			1.89e-04 ± 6.5e-05	3.177e-03 ± 3.9e-05	4.448e-04 ± 5.4e-06	4.05e-04	4.7e-02 ± 1.6e-02
42MeV Scan			-4.e-05 ± 1.6e-04	-2.885e-03 ± -1.2e-05	-4.039e-04 ± -1.7e-06	4.05e-04	-1.3e-02 ± -5.6e-02
38MeV Scan			-6.7e-05 ± 3.0e-05	-3.474e-03 ± -3.8e-05	-4.400e-04 ± -4.8e-06	4.05e-04	-1.92e-02 ± -8.7e-03
47MeV Scan			-1.01e-04 ± 6.0e-05	-2.588e-03 ± -1.2e-05	-4.055e-04 ± -1.8e-06	4.05e-04	-3.9e-02 ± -2.3e-02
53MeV Scan			-4.7e-05 ± 4.5e-05	-2.2839e-03 ± -1.0e-05	-4.035e-04 ± -1.8e-06	4.05e-04	-2.0e-02 ± -2.0e-02

Table 10

Characterization Table of MS1CRV01 at IS1BPM01

	Bend angle (horizontal) at Nominal Current [Radians]	Bend angle (vertical) at Nominal Current [Radians]	Horizontal Bend Angle / Current [Radians/Amp]	Vertical Bend Angle / Current [Radians/Amp]	Calibration Value [Tesla Meters/Amp]	Expected Field Integral Along Trajectory [Tesla Meters/Amp]	Roll Angle [Radians]
42MeV Quads Off	-1.e-03 ± 2.5e-03	6.63e-03 ± 2.1e-04	-6.e-04 ± 1.6e-03	4.07e-03 ± 1.3e-04	5.69e-04 ± 1.8e-05	4.05e-04	-1.1e-01 ± -3.0e-01
42MeV Scan	-9.6e-04 ± 2.7e-04	-4.406e-03 ± -4.2e-05	-5.9e-04 ± 1.6e-04	-2.702e-03 ± -2.6e-05	-3.783e-04 ± -3.6e-06	4.05e-04	-1.72e-01 ± -4.8e-02
38MeV Scan	-5e-06 ± 1.4e-04	-5.153e-03 ± -2.8e-05	-3.e-06 ± 8.4e-05	-3.160e-03 ± -1.7e-05	-4.003e-04 ± -2.1e-06	4.05e-04	-8.e-04 ± -2.1e-02
47MeV Scan	3.4e-04 ± 1.8e-04	-4.052e-03 ± -3.2e-05	2.1e-04 ± 1.1e-04	-2.485e-03 ± -2.0e-05	-3.894e-04 ± -3.1e-06	4.05e-04	6.7e-02 ± 3.4e-02
53MeV Scan	3.3e-04 ± 1.4e-04	-3.705e-03 ± -1.7e-05	2.01e-04 ± 8.7e-05	-2.272e-03 ± -1.1e-05	-4.014e-04 ± -1.9e-06	4.05e-04	7.0e-02 ± 3.0e-02

Table 11

Characterization Table of MS1CRV02 at IS1BPM02

	Bend angle (horizontal) at Nominal Current [Radians]	Bend angle (vertical) at Nominal Current [Radians]	Horizontal Bend Angle / Current [Radians/Amp]	Vertical Bend Angle / Current [Radians/Amp]	Calibration Value [Tesla Meters/Amp]	Expected Field Integral Along Trajectory [Tesla Meters/Amp]	Roll Angle [Radians]
42MeV Quads Off			-4.e-05 ± 1.2e-04	2.990e-03 ± 2.4e-05	4.186e-04 ± 3.4e-06	4.05e-04	-1.e-02 ± -3.1e-02
42MeV Scan			8.3e-05 ± 8.1e-05	-2.861e-03 ± -2.3e-05	-4.006e-04 ± -3.2e-06	4.05e-04	1.8e-02 ± 1.7e-02
38MeV Scan			-6.2e-05 ± 4.4e-05	-2.876e-03 ± -1.4e-05	-3.643e-04 ± -1.7e-06	4.05e-04	-1.32e-02 ± -9.5e-03
47MeV Scan			-2.3e-04 ± 2.9e-04	-2.654e-03 ± -2.2e-05	-4.157e-04 ± -3.4e-06	4.05e-04	-5.2e-02 ± -6.7e-02
53MeV Scan			2.2e-05 ± 4.8e-05	-2.3683e-03 ± -7.9e-06	-4.184e-04 ± -1.4e-06	4.05e-04	6.e-03 ± 1.2e-02

Table 12

Characterization Table of MS1CRV03 at IS1BPM06

	Bend angle (horizontal) at Nominal Current [Radians]	Bend angle (vertical) at Nominal Current [Radians]	Horizontal Bend Angle / Current [Radians/Amp]	Vertical Bend Angle / Current [Radians/Amp]	Calibration Value [Tesla Meters/Amp]	Expected Field Integral Along Trajectory [Tesla Meters/Amp]	Roll Angle [Radians]
42MeV Quads Off	NA	NA	NA	NA	NA	4.05e-04	NA
42MeV Scan			-4.9e-05 ± 3.8e-05	-3.295e-03 ± -4.0e-05	-4.613e-04 ± -5.7e-06	4.05e-04	-2.2e-02 ± -1.7e-02
38MeV Scan			-6.7e-05 ± 3.2e-05	-5.43e-04 ± -2.6e-05	-6.87e-05 ± -3.3e-06	4.05e-04	-1.84e-01 ± -8.9e-02
47MeV Scan			-1.9e-04 ± 1.3e-04	-4.85e-03 ± -2.4e-04	-7.61e-04 ± -3.8e-05	4.05e-04	-5.9e-02 ± -4.0e-02
53MeV Scan			-7.3e-05 ± 3.6e-05	-5.669e-03 ± -2.1e-05	-1.0016e-03 ± -3.8e-06	4.05e-04	-1.92e-02 ± -9.4e-03

Table 13

Characterization Table of MS1CRV04 at IFABPM01

Appendix C: Cubic Fit to Nonlinear BPM Measurements in Direction of Design

Of many more BPM readings, the following are the closest-downstream BPM readings, which are used to characterize each magnet. The following plots are in the direction of designed kick, that is slope of horizontal position measurements for dipoles and slope of vertical position measurements for vertical correctors.

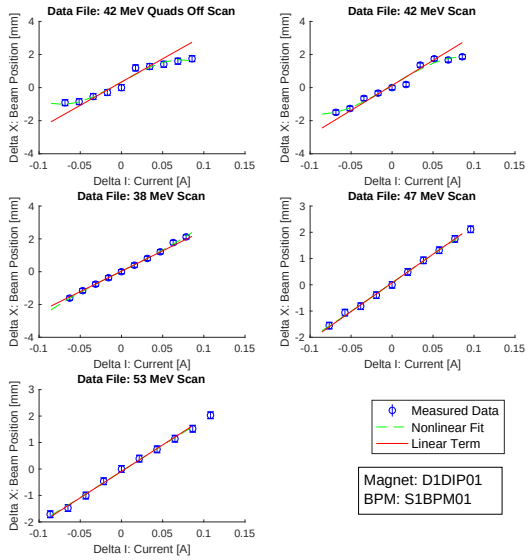

Figure 19. Cubic fit of MD1DIP01 read at IS1BPM01. For the datasets 42MeV Quads Off, 42MeV Scan, 38MeV Scan, 47MeV Scan, and 53MeV Scan, χ^2 = 0.33974, 0.39467, 0.013374, 0.025614, and 0.04236 respectively.

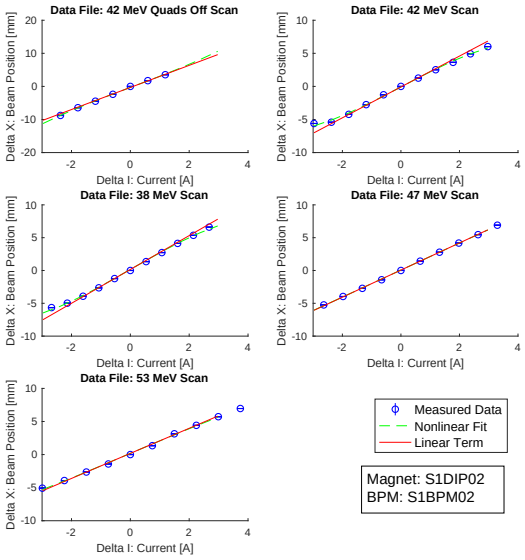

Figure 20. Cubic fit of MS1DIP02 read at IS1BPM02. For the datasets 42MeV Quads Off, 42MeV Scan, 38MeV Scan, 47MeV Scan, and 53MeV Scan, χ^2 = 0.15898, 0.42851, 0.30339, 0.044351, and 0.21801 respectively.

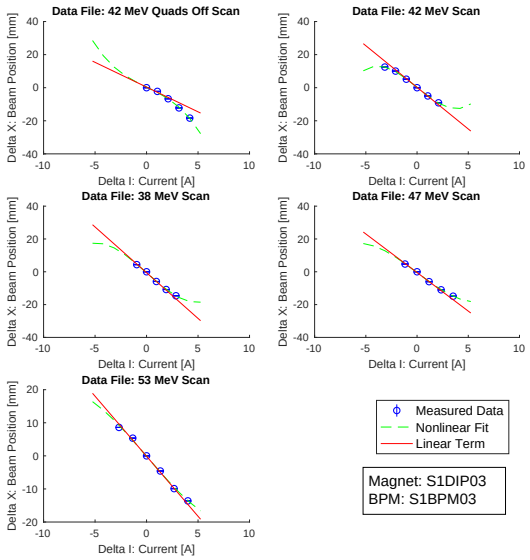

Figure 21. Cubic fit of MS1DIP03 read at IS1BPM03. For the datasets 42MeV Quads Off, 42MeV Scan, 38MeV Scan, 47MeV Scan, and 53MeV Scan, χ^2 = 0.80844, 0.22256, 0.46714, 0.31036, and 1.1787 respectively.

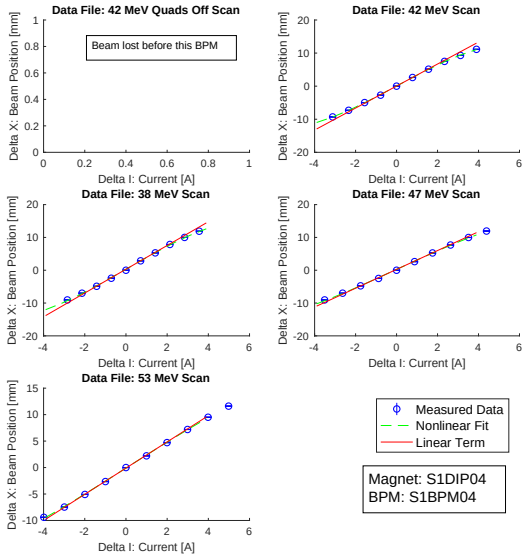

Figure 22. Cubic fit of MS1DIP04 read at IS1BPM04. For the datasets 42MeV Scan, 38MeV Scan, 47MeV Scan, and 53MeV Scan, χ^2 =0.072409, 0.2519, 0.26597, and 0.12563 respectively.

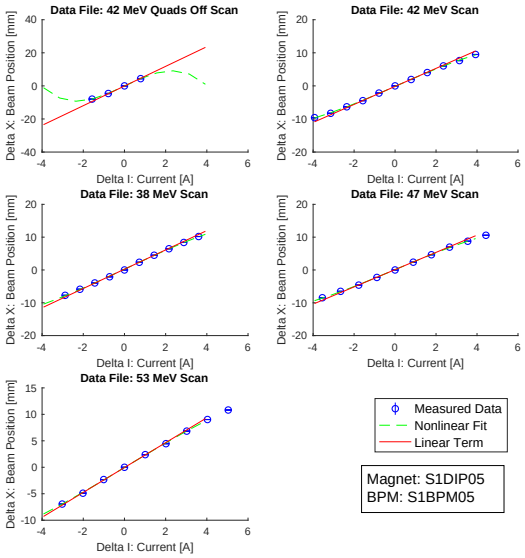

Figure 23. Cubic fit of MS1DIP05 read at IS1BPM05. For the datasets 42MeV Quads Off, 42MeV Scan, 38MeV Scan, 47MeV Scan, and 53MeV Scan, χ^2 =0.0095202, 0.1273, 0.1341, 0.083928, and 0.088286 respectively.

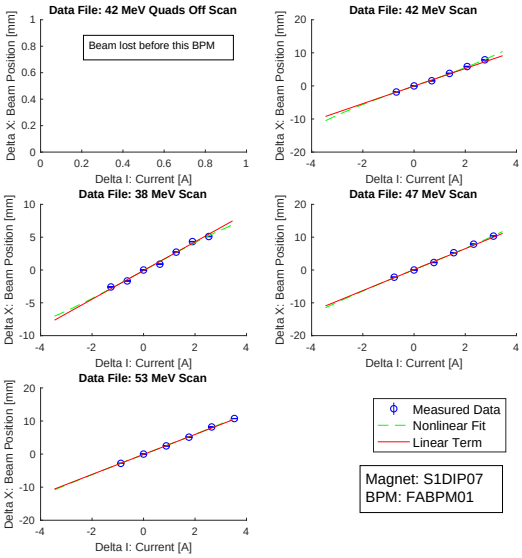

Figure 25. Cubic fit of MS1DIP07 read at IFABPM01. For the datasets 42MeV Scan, 38MeV Scan, 47MeV Scan, and 53MeV Scan, χ^2 = 0.084611, 0.41489, 0.19916, and 0.084758 respectively.

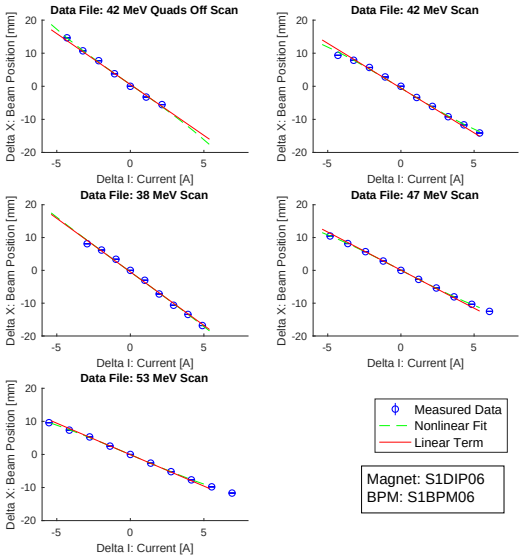

Figure 24. Cubic fit of MS1DIP06 read at IS1BPM06. For the datasets 42MeV Quads Off, 42MeV Scan, 38MeV Scan, 47MeV Scan, and 53MeV Scan, χ^2 =1.182, 2.1229, 2.6277, 0.032095, and 0.074218 respectively.

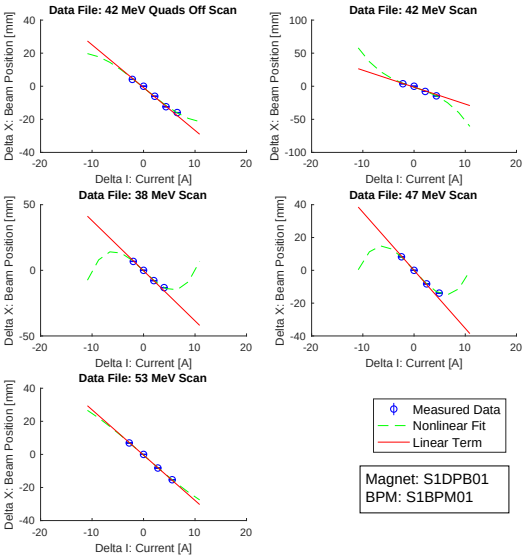

Figure 26. Cubic fit of MS1DPB01 read at IS1BPM01. For the datasets 42MeV Quads Off, 42MeV Scan, 38MeV Scan, 47MeV Scan, and 53MeV Scan, χ^2 = 1.7908, 2.769, 0.18375, 4.2667e-05, and 0.28908 respectively.

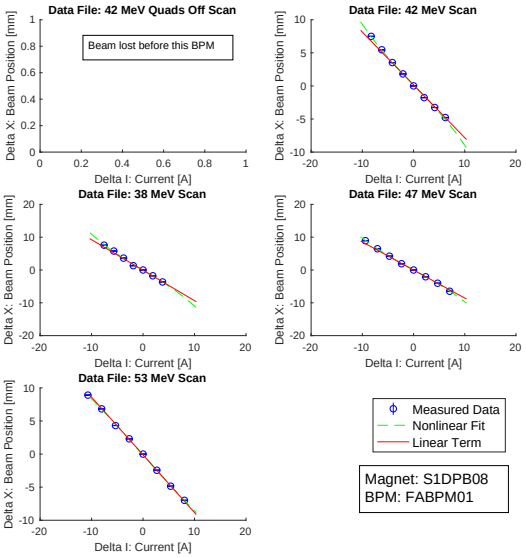

Figure 27. Cubic fit of MS1DPB08 read at IFABPM01. For the datasets 42MeV Scan, 38MeV Scan, 47MeV Scan, and 53MeV Scan, χ^2 = 0.19319, 0.2484, 0.040289, and 0.077736 respectively.

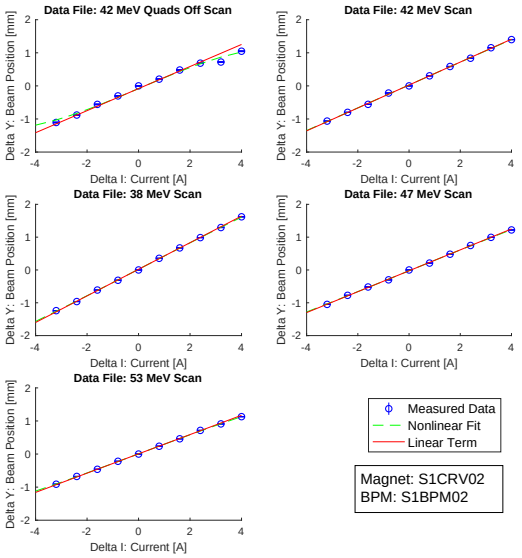

Figure 29. Cubic fit of MS1CRV02 read at IS1BPM02. For the datasets 42MeV Quads Off, 42MeV Scan, 38MeV Scan, 47MeV Scan, and 53MeV Scan, χ^2 = 0.043047, 0.0039905, 0.0017472, 0.0023514, and 0.0006721 respectively.

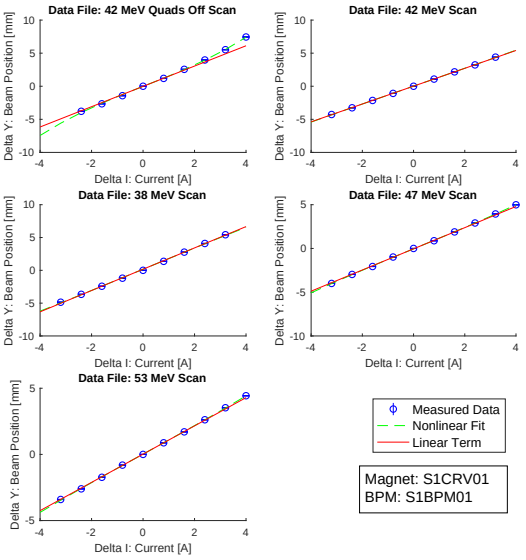

Figure 28. Cubic fit of MS1CRV01 read at IS1BPM01. For the datasets 42MeV Quads Off, 42MeV Scan, 38MeV Scan, 47MeV Scan, and 53MeV Scan, χ^2 = 0.081223, 0.0072403, 0.07261, 0.011177, and 0.0080622 respectively.

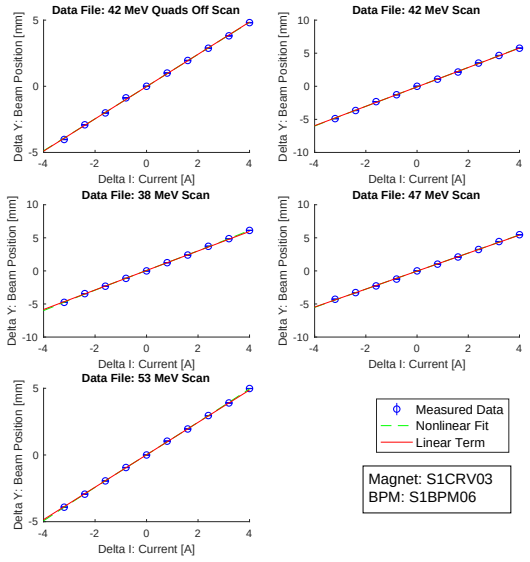

Figure 30. Cubic fit of MS1CRV03 read at IS1BPM06. For the datasets 42MeV Quads Off, 42MeV Scan, 38MeV Scan, 47MeV Scan, and 53MeV Scan, χ^2 = 0.036884, 0.051184, 0.017873, 0.045062, and 0.0061283 respectively.

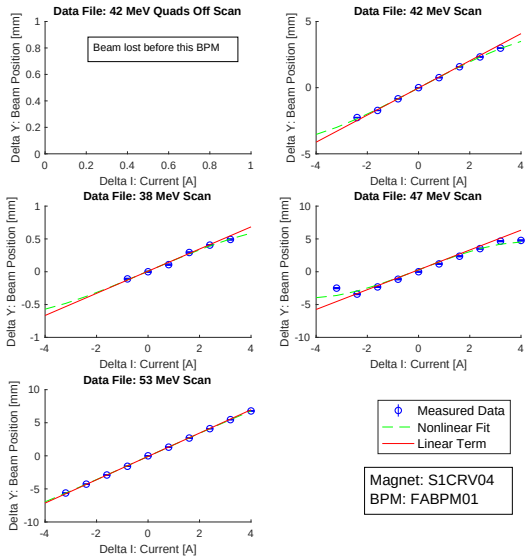

Figure 31. Cubic fit of MS1CRV04 read at IFABPM01. For the datasets 42MeV Scan, 38MeV Scan, 47MeV Scan, and 53MeV Scan, χ^2 = 0.021291, 0.0022139, 2.1151, and 0.016398 respectively.

Appendix D: Cubic Fit to Nonlinear BPM Measurements in Direction Perpendicular to Design

The following are the closest-downstream BPM readings used to characterize each magnet in the direction perpendicular to designed kick, that is slope of vertical position measurements for dipoles and slope of horizontal position measurements for vertical correctors.

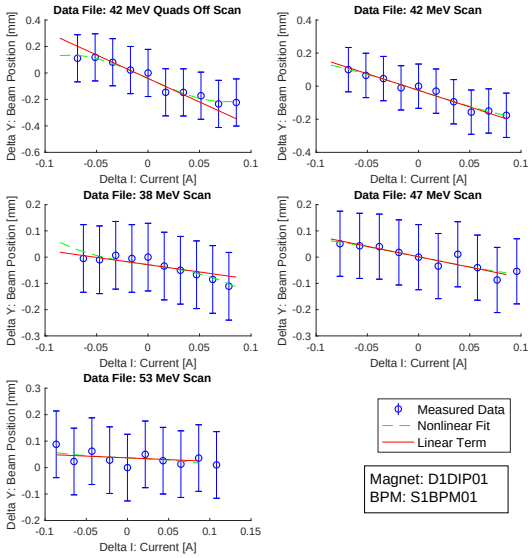

Figure 32. Cubic fit of MD1DIP01 read at IS1BPM01. For the datasets 42MeV Quads Off, 42MeV Scan, 38MeV Scan, 47MeV Scan, and 53MeV Scan, χ^2 = 0.0053786, 0.0030422, 0.0023649, 0.0032671, and 0.004281 respectively.

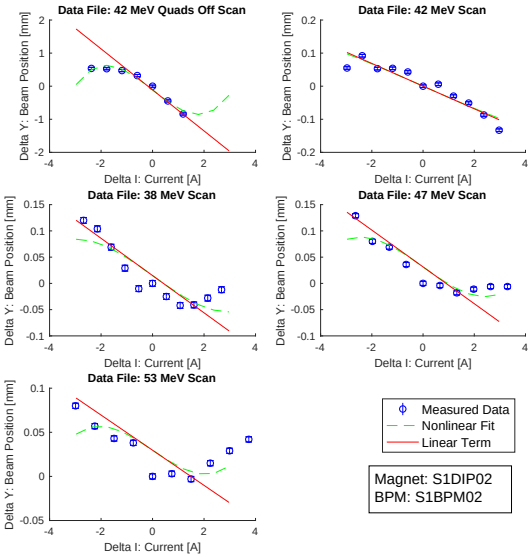

Figure 33. Cubic fit of MS1DIP02 read at IS1BPM02. For the datasets 42MeV Quads Off, 42MeV Scan, 38MeV Scan, 47MeV Scan, and 53MeV Scan, χ^2 = 0.042603, 0.0049244, 0.0076858, 0.0038359, and 0.0027939 respectively.

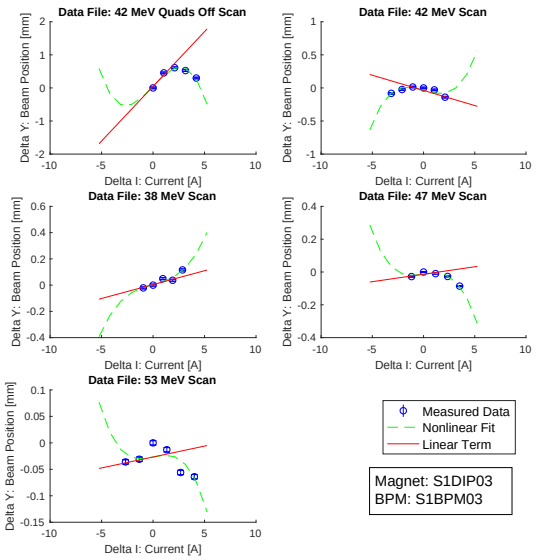

Figure 34. Cubic fit of MS1DIP03 read at IS1BPM03. For the datasets 42MeV Quads Off, 42MeV Scan, 38MeV Scan, 47MeV Scan, and 53MeV Scan, χ^2 = 0.014677, 0.0083964, 0.0010303, 0.00026654, and 0.0016079 respectively.

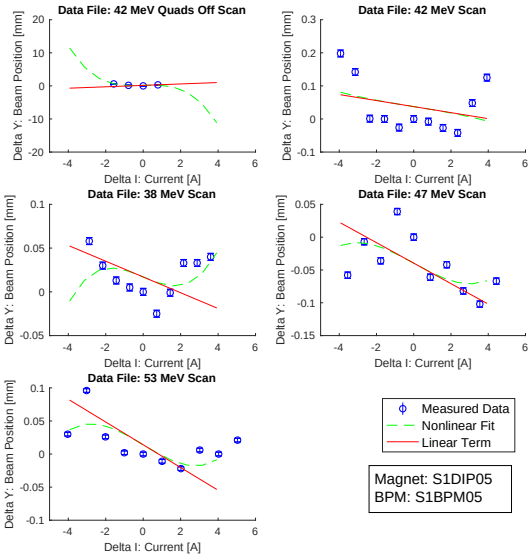

Figure 36. Cubic fit of MS1DIP05 read at IS1BPM05. For the datasets 42MeV Quads Off, 42MeV Scan, 38MeV Scan, 47MeV Scan, and 53MeV Scan, χ^2 = 0.036974, 0.05769, 0.0047361, 0.010392, and 0.0045855 respectively.

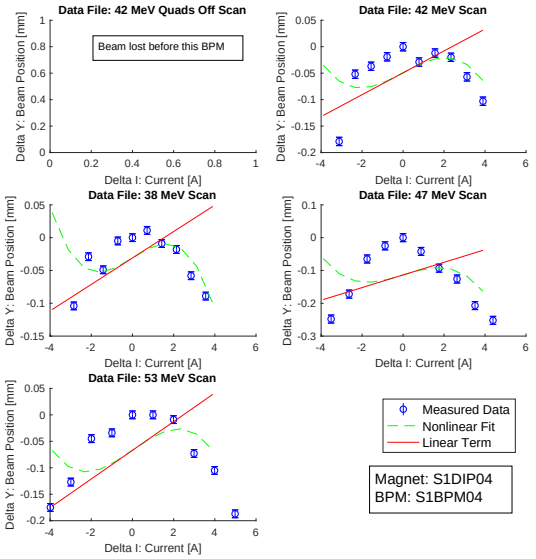

Figure 35. Cubic fit of MS1DIP04 read at IS1BPM04. For the datasets 42MeV Scan, 38MeV Scan, 47MeV Scan, and 53MeV Scan, χ^2 = 0.021839, 0.010182, 0.06651, and 0.031073 respectively.

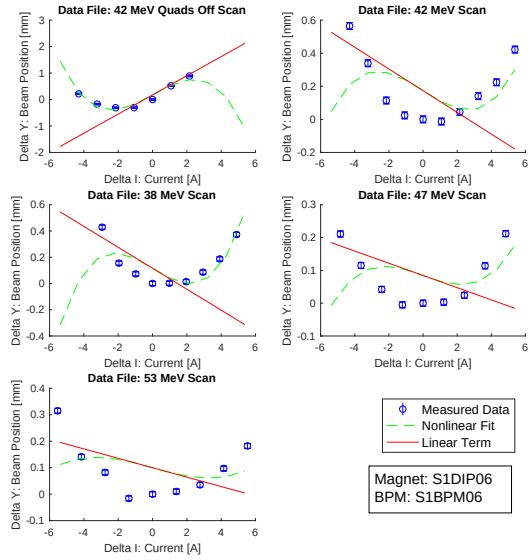

Figure 37. Cubic fit of MS1DIP06 read at IS1BPM06. For the datasets 42MeV Quads Off, 42MeV Scan, 38MeV Scan, 47MeV Scan, and 53MeV Scan, χ^2 = 0.089737, 0.27772, 0.089096, 0.069825, and 0.092489 respectively.

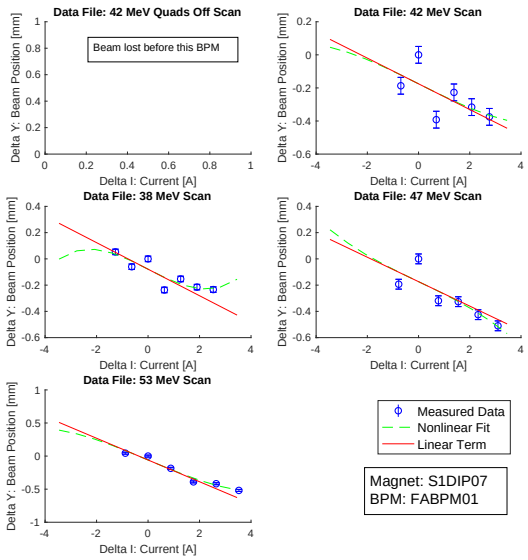

Figure 38. Cubic fit of MS1DIP07 read at IFABPM01. For the datasets 42MeV Scan, 38MeV Scan, 47MeV Scan, and 53MeV Scan, χ^2 = 0.064612, 0.019376, 0.044103, and 0.0091475 respectively.

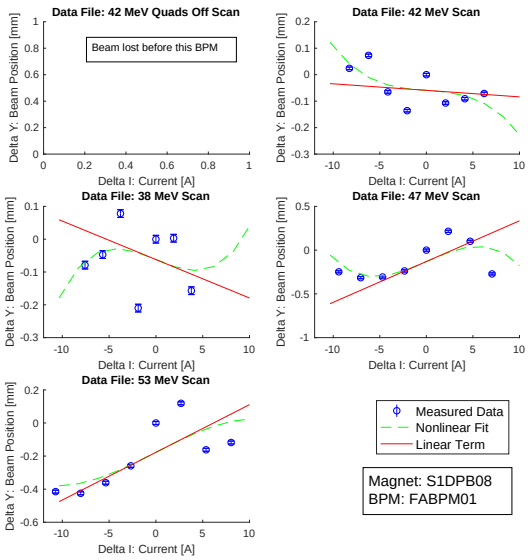

Figure 40. Cubic fit of MS1DPB08 read at IFABPM01. For the datasets 42MeV Scan, 38MeV Scan, 47MeV Scan, and 53MeV Scan, χ^2 = 0.021545, 0.055357, 0.17694, and 0.11905 respectively.

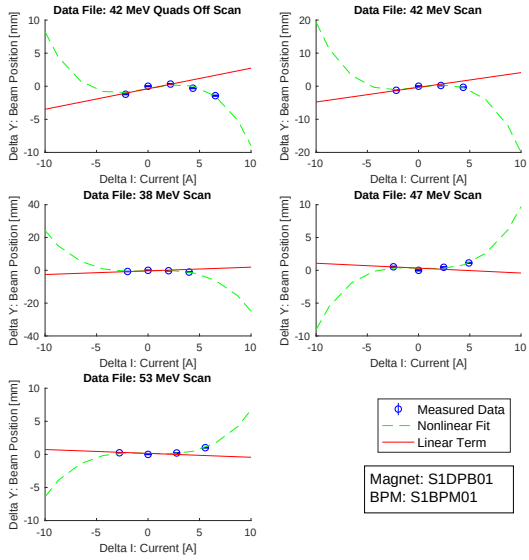

Figure 39. Cubic fit of MS1DPB01 read at IS1BPM01. For the datasets 42MeV Quads Off, 42MeV Scan, 38MeV Scan, 47MeV Scan, and 53MeV Scan, χ^2 = 0.35646, 0.17137, 0.15424, 0.16633, and 0.03542 respectively.

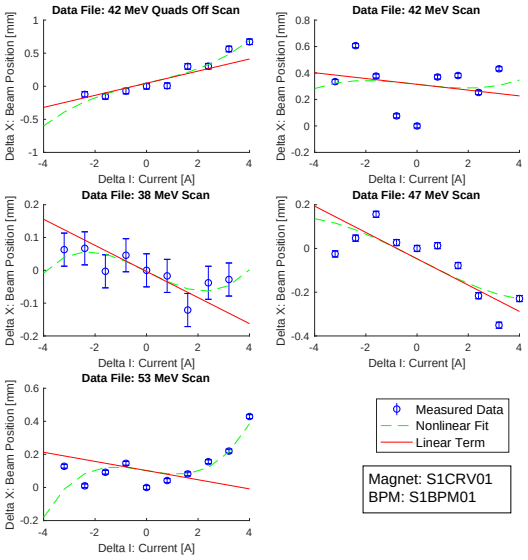

Figure 41. Cubic fit of MS1CRV01 read at IS1BPM01. For the datasets 42MeV Quads Off, 42MeV Scan, 38MeV Scan, 47MeV Scan, and 53MeV Scan, χ^2 = 0.046162, 0.26715, 0.0092283, 0.073055, and 0.04148 respectively.

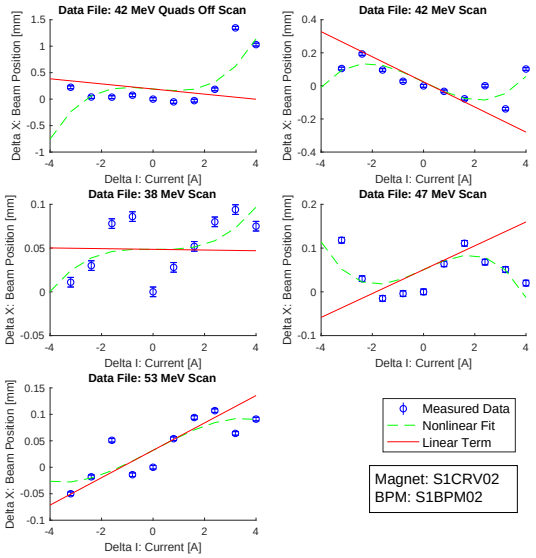

Figure 42. Cubic fit of MS1CRV02 read at IS1BPM02. For the datasets 42MeV Quads Off, 42MeV Scan, 38MeV Scan, 47MeV Scan, and 53MeV Scan, χ^2 = 0.94619, 0.025981, 0.0068628, 0.011295, and 0.0073278 respectively.

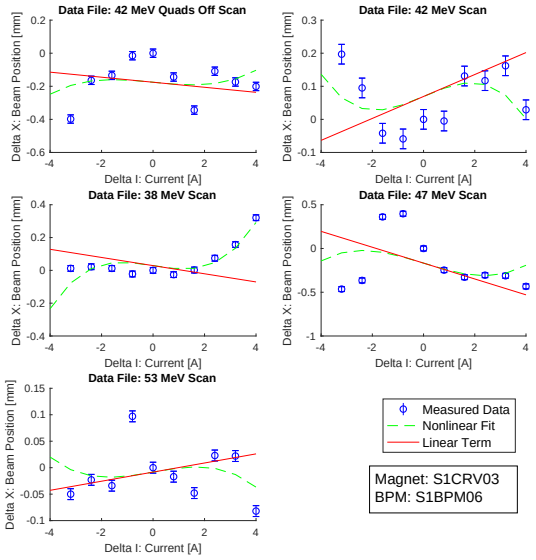

Figure 43. Cubic fit of MS1CRV03 read at IS1BPM06. For the datasets 42MeV Quads Off, 42MeV Scan, 38MeV Scan, 47MeV Scan, and 53MeV Scan, χ^2 = 0.13553, 0.060744, 0.018223, 0.78518, and 0.021531 respectively.

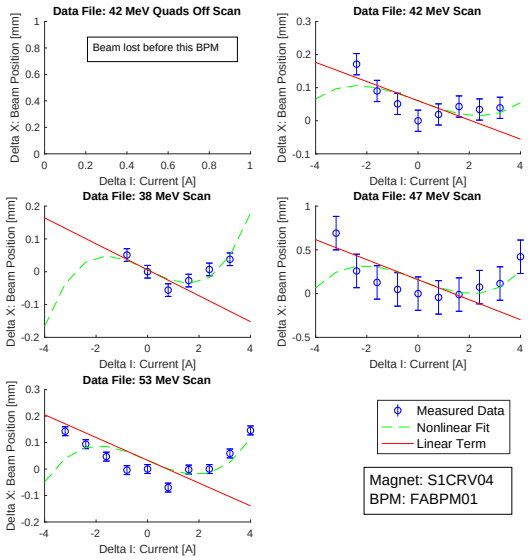

Figure 44. Cubic fit of MS1CRV04 read at IFABPM01. For the datasets 42MeV Scan, 38MeV Scan, 47MeV Scan, and 53MeV Scan, χ^2 = 0.010395, 0.0021801, 0.349, and 0.025661 respectively.